Generation of controlled irregular wave crest statistics in experimental and numerical wave tanks

Maxime Canard, Guillaume Ducrozet, Benjamin Bouscasse

Ocean Engineering 310 (2024) 118676

Contents lists available at ScienceDirect

Ocean Engineering

journal homepage: www.elsevier.com/locate/oceaneng

Generation of controlled irregular wave crest statistics in experimental and numerical wave tanks

Maxime Canard, Guillaume Ducrozet *, Benjamin Bouscasse

Nantes Université, École Centrale Nantes, CNRS, LHEEA, UMR 6598, F-44000 Nantes, France

ARTICLE INFO

Keywords:
Wave tank experiment
Numerical wave tank
Wave energy spectrum
Wave creststatistics
Wave generation
Nonlinear waves

ABSTRACT

In the context of ocean engineering studies or ocean wave physics research, irregular wave fields are generated in experimental and numerical wave tanks. In these environments, a wave maker generates the waves and the wave field is studied at a target position X_t, further in the tank. Therefore, the properties of the wave fields need to be controlled at X_t. The state-of-the-art wave generation procedures focus on accurately generating a target wave energy spectrum. However, the wave field is also characterized by its statistical features (crest height distribution, free surface elevation probability density function) that cannot be retrieved from the wave spectrum. To tackle this issue, the present paper introduces a new wave generation procedure that makes use of the natural spatial evolution of the wave statistics to generate at any target location X_t a controlled spectrum and a controlled crest distribution. The procedure is tested experimentally and numerically. The results validate the methodology for non-breaking unidirectional wave conditions, for experimental, numerical, and hybrid numerical/experimental configurations.

1. Introduction

In the design stage of ships and offshore structures, sea-keeping tests are performed to assess their response to specific wave conditions defined by classification societies. The tests are conducted in experimental or numerical wave tanks, at a model scale relying on the Froude Similitude.

Different types of wave conditions exist. The generated wave field can be monochromatic (regular waves) or polychromatic (irregular waves, representative of the ocean). The sea state is described in the frequency domain with the wave energy spectrum $S(f)$ (f being the frequency) or with the directional spectrum $S(f,\theta)$ (θ being the direction). Consequently, the most realistic sea-keeping tests are based on irregular wave fields, generated to reproduce the so-called design spectra $S_{\text{design}}(f)$, specific to the geographical area where the ship or structure is to be deployed (Bureau Veritas, 2019). In ocean engineering, a design procedure usually assesses the response of the structure to the incoming waves. It consists in evaluating the most extreme event that is expected for a given probability P_{design}, and this for each tested wave spectrum. Wave-related events are commonly defined with extrema observed between zero-upcrossings computed either on the response time history or on the incident wave time history. The typical duration considered for a sea state is 3 h at full scale. This means that with a typical wave period ($T \approx 10$ s), the most extreme event to be analyzed approximatively occurs once every 10^3 events, which corresponds to a design probability of the order of $P_{\text{design}} = 10^{-3}$.

To generate a design sea state in a wave tank (in model-scale experiments or with numerical simulations), two main methodologies are used by the ocean engineering community. The first approach, which is the most straightforward, is stochastic (ITTC, 2011; Det Norske Veritas, 2010). Long-duration realizations are generated, based on the design spectrum and random phases, possibly associated with random amplitudes. The duration and number of realizations are selected in such a way that the statistical features of the total wave field, considering all realizations, are statistically converged at the probability of interest P_{design}. It corresponds to a total run duration far larger than T/P_{design} (van Essen et al., 2023). Typically 10 to 30 realizations of duration $\approx T/P_{\text{design}}$ are generated. For typical P_{design}, T, and model scale values at use in ocean engineering, T/P_{design} is approximately equal to 3 h at full scale and 20 min at model scale.

Second, the response of the model facing a design sea state can also be assessed through a deterministic approach. Only selected events are tested instead of generating long-duration wave fields. Their shape is meticulously designed to be representative of given (S_{design}, P_{design}) couples. See for instance the "New Wave method" (Tromans et al., 1991), providing the most probable linear wave profile at a certain probability; the FORM (first-order reliability method), solving a minimization problem to provide the wave profile and the associated

* Corresponding author.
E-mail address: guillaume.ducrozet@ec-nantes.fr (G. Ducrozet).

https://doi.org/10.1016/j.oceaneng.2024.118676
Received 7 March 2024; Received in revised form 30 May 2024; Accepted 4 July 2024
Available online 18 July 2024

probability (even if the response distribution is not known) (Jensen and Capul, 2006); or the EDW method (equivalent design waves), based on a FORM approach coupled with a nonlinear wave solver (Kim et al., 2022). Recently, a hybrid deterministic/stochastic methodology has also been developed in Huo et al. (2023), allowing to directly generate the most extreme events of a given sea state without generating a long duration wave field. However, the present paper focuses on the stochastic approach and will not address these deterministic methodologies. Also, we consider only deep-water waves ($k_p d > \pi$, with k_p the peak wavenumber and d the depth), and unidirectional propagation.

To assess the quality of a generated stochastic wave field in an experimental or numerical wave tank, classification societies (Det Norske Veritas, 2010), research groups (Fouques et al., 2021), and other international organizations such as the International Towing Tank Conference (ITTC, 2011) have defined qualification criteria. They apply to the stochastic quantities computed from the measured wave field at the location of interest in the tank, referred to as the target location X_t, which is the distance from the wave maker. For a wave-structure interaction study with a fixed or moored object, X_t is the position of the model. These state-of-the-art qualification methodologies consist in assessing the quality of the wave spectrum at X_t before comparing the crest height distribution to theoretical and semi-empirical references.

Generating a qualified sea state at X_t is not straightforward. The most fundamental stochastic wave generation procedure is to take as input for the wave maker free-surface elevation time sequences, $\eta_{\text{input}}(t)$, built with $S_{\text{design}}(f)$ and random phases (see more details in Appendix A). The $\eta_{\text{input}}(t)$ statistical distribution is Gaussian. The corresponding crest height distribution follows a Rayleigh-type shape that mainly depends on the spectrum width (see for instance (Longuet-Higgins, 1952; Tayfun and Fedele, 2007)). Then, if considering linear wave propagation without dissipation and a perfect wave maker, the wave field measured at X_t is also Gaussian and its spectrum (labeled as $S(f, X_t)$) perfectly matches $S_{\text{design}}(f)$. However, for practical applications to design sea states and wave tanks, this is not the case.

First, wave propagation is not linear. The frequency components of the wave field interact with each other. The non-linearity affects the wave spectrum and the statistics in various ways. Mainly, second-order nonlinear interactions lead to bound waves, making crests sharper and troughs flatter. This shifts the crest distribution towards larger values. Theoretical (Tayfun, 1990) and semi-empirical (Forristall, 2000) references account for this phenomenon, which is uniformly present throughout the domain. Its magnitude is driven by the wave steepness that is computed as $\epsilon_p = H_s/\lambda_p$, with λ_p the peak wavelength and H_s the significant wave height. In addition, for steep and narrow-band spectra the third-order nonlinear interactions known as 'Benjamin Feir instabilities' modulate the wave envelope (Benjamin and Feir, 1967). The disposition of the sea states to develop such instabilities can be quantified by the Benjamin Feir Index (BFI), the ratio between the steepness and the non-dimensional spectral width, introduced in Janssen (2003). The definition used in this paper and the computational methodology were suggested in Serio et al. (2005) and is provided in Appendix B.

In a wave tank configuration, these high-order nonlinear interactions induce evolution in space of the spectrum and the crest distribution. This was extensively observed in experiments, see for instance (Onorato et al., 2006; Cherneva et al., 2009; Fedele et al., 2010). These studies showed that, as the waves propagate along the tank, the spectrum broadens and the probability of large crest heights increases. The intensity of these phenomena diminishes for multidirectional waves (Onorato et al., 2009), and breaking conditions (Karmpadakis and Swan, 2022). The effect of the water depth was also explored, see Karmpadakis et al. (2019), Tang and Adcock (2021), Zve et al. (2023). For intermediate depths, small $k_p d$ values reduce the modulational instabilities. However, they amplify the second-order bound waves. The crest distribution is therefore influenced by these two competing effects.

Besides, the spectrum and crest distribution are affected by dissipation mechanisms. In long and narrow wave tanks, the sidewall friction dissipates the energy of the waves. In intermediate water depth conditions ($k_p d \in [\pi/10, \pi]$), the bottom of the tank also contributes to the dissipation. An analytical model of this phenomenon is provided in Henderson et al. (2015). Moreover, for sea states exhibiting high steepness, breaking events appear, reducing the amplitude of the most extreme crests and dissipating some energy (Onorato et al., 2006; Latheef and Swan, 2013).

To generate a qualified wave field despite the complex wave propagation, the state-of-the-art generation procedures correct the spectrum at X_t, iterating on the wave-maker inputs to balance dissipation and nonlinear effects (Fouques et al., 2021). Note that in experiments, the iterations also correct the possible lack of accuracy of the wave maker transfer function, and the influence of the spurious waves (reflected waves, transverse modes). Iterating on the wave-maker inputs to correct the spectrum at X_t, Canard et al. (2022b) generated the same design spectrum at several locations over a long wave tank. It was found that the same qualified spectrum can be associated with various statistical behaviors depending on the target location, due to the spatial evolution of the wave statistics, induced mostly by the modulational instabilities. This demonstrated that qualifying the spectrum is not enough to control the crest distribution, at least in configurations where the modulational instabilities are prominent (unidirectional waves, moderate to large BFI value, and nonbreaking conditions). Specifically, when targeting a design spectrum at a location larger than 20 peak wavelengths (λ_p) from the wave maker, the distribution shows impressively large probabilities for extreme crest heights, not predicted by the typical reference probability distributions used for ocean engineering studies.

In this paper, we propose a new wave generation procedure that allows for controlling both the spectrum and the crest distribution at any specific location in the tank X_t. The procedure is validated experimentally using the Ecole Centrale Nantes (ECN) facilities and numerically with the nonlinear potential wave-solver `HOS-NWT`. The paper is organized into four sections in addition to this introduction. First, the different tools used in this study are presented, including the ECN experimental facilities and the numerical wave tank solver `HOS-NWT`. Then, after providing the studied wave conditions, Section 3 briefly presents the spatial evolution of the wave field when using state-of-the-art generation procedures. Next, Section 4 introduces the new wave generation procedure studied in this paper, which allows for controlling both the spectrum and the crest distribution at X_t. Section 5 provides the experimental and numerical validation of the procedure. Finally, Section 6 concludes the paper.

2. Experimental and numerical wave tank

This section describes the experimental facilities and the numerical tool used in this paper. The new methodology proposed in Section 4 to control both the wave spectrum and the wave statistics can be implemented in both contexts. They were used for validation purposes in Section 5 and represent the main applications of the procedure developed.

2.1. Experiments

Experiments were performed in two ECN facilities,[1] namely the Ocean Engineering tank (O.E. tank) and the Towing tank (T. tank). Fig. 1 presents photos of the two tanks. We note x and y the longitudinal and the transverse coordinates in the horizontal plane, while z stands for the vertical coordinate pointing upwards.

[1] https://lheea.ec-nantes.fr/english-version/test-facilities

(a) Towing tank (b) Ocean Engineering tank

Fig. 1. Photos of the ECN facilities.

The O.E. tank is a large rectangular basin (50 m × 30 m × 5 m) equipped with a 48-paddle wave maker (single hinge located 2.15 m from the bottom) on one side ($x = 0$). It is designed to generate unidirectional and multidirectional deep-water sea states. Its capabilities cover periods from 0.5 to 5.0 s and significant wave heights H_s up to 0.8 m. The Towing tank is a long channel (140 m × 5 m × 2.8 m) equipped with a one-flap wave maker (single hinge located at 0.47 m from the bottom) that can generate wave periods from 0.5 s to 5 s and significant wave heights up to 0.3 m. A moving carriage can be set up to perform towing experiments and measure ship resistance. The latter was not used in the present wave-only study. The passive absorbing system of the facilities was studied in Bonnefoy (2005). The reflection coefficients, in terms of wave amplitude, do not exceed 5 to 10% within the range of frequencies covered by the wave makers.

For both tanks, the wave maker is mechanically limited to oscillatory motions with frequencies below 2 Hz. Its motion is defined through the corresponding free surface elevation $\eta_{\text{input}}(t)$ at its location ($x = 0$) associated with a linear transfer function. A ramp in time is applied to the motion at the beginning and the end of the experiments to prevent mechanical issues. Its duration was set to 10 seconds for the present study.

In the experiments analyzed in this paper, networks of resistive wave gauges were installed to provide time series data of the free-surface elevation at specific single-point positions, $\eta(t, x_{\text{meas}})$. Fig. 2 shows their position in the two tanks. To analyze the recorded data, one must choose the appropriate time windows that remove the non-stationary development of the wave field at the probe location. The sea state generated for the present study is characterized by an energy spectrum centered around a peak frequency f_p and containing most of energy up to $2f_p$ (see Section 3.1). Then, for each probe, we used the following analysis window, depending on the probe position x_{meas}:

$$t_{\text{beg}} = x_{\text{meas}}/c_g(2f_p) \tag{1}$$

$$t_{\text{end}} = \Delta T + x_{\text{meas}}/c_g(2f_p) \tag{2}$$

with $c_g(2f_p)$ the group velocity at twice the peak frequency, and ΔT a duration, constant for all the probes, fixed as $\Delta T \leq T_{\text{WVMK}} - \max(x_{\text{meas}})/c_g(2f_p)$ (T_{WVMK} is the time at which the wave maker stops, and $\max(x)$ denotes the position of the furthest probe in the network). This procedure allows for the analysis of an equal duration (*i.e.* number of waves) at each probe location.

Each stochastic quantity Q, computed from the measured free-surface elevation series $\eta(t, x_{\text{meas}})$ is affected by uncertainties. In this paper, we distinguish the *measurement uncertainty* $u_s^{\text{meas}}(Q)$ i.e. the differences between the recorded data and the occurring waves, and the *sampling variability* $u_s^{\text{samp}}(Q)$ i.e. the differences between the statistically converged quantities and the ones computed with a limited number of data. Note that the sampling variability also affects the numerical results. $u_s^{\text{meas}}(\eta)$ was estimated using the wave gauge calibration bench relying on (ITTC, 2017) guidance. Depending on the wave gauge, $u_s^{\text{meas}}(\eta)$ ranges from 1 to 2 mm, which corresponds to 2 to 4% of the significant wave height of the generated design sea state. $u_s^{\text{meas}}(Q)$ was then estimated for each quantity using the standard uncertainty propagation laws (see guidelines in ITTC (2008), ISO/IEC (2008)). Complementary $u_s^{\text{samp}}(Q)$ was estimated with convergence studies or confidence intervals for the spectrum and crest distribution (using respectively the Welch (Welch, 1967) and Jeffrey (Brown et al., 2001) 95% confidence intervals).

In the presented results u_s^{meas} is always plotted with error bars. Complementary, the total uncertainty range for each quantity Q,

$$u_s(Q) = \sqrt{u_s^{\text{meas}}(Q)^2 + u_s^{\text{samp}}(Q)^2} \tag{3}$$

is displayed with a dedicated shaded area. The comparison between realizations built with the same set of random phases shows that the sampling variability does not affect the comparison, therefore, only u_s^{meas} is plotted.

2.2. Numerical simulations

2.2.1. HOS-NWT solver

Unidirectional numerical-wave-tank (NWT) simulations were conducted using the HOS-NWT solver, which is developed by ECN and released open-source.[2] A comprehensive description of the code is provided for instance in Ducrozet et al. (2012). This solver is based on nonlinear potential flow theory. It solves the dynamic and kinematic free-surface boundary conditions, using the High-Order Spectral method (Dommermuth and Yue, 1987; West et al., 1987). It incorporates nonlinear features of water wave propagation up to an arbitrary order of nonlinearity M. The numerical solution is obtained thanks to a pseudo-spectral method. The unknowns are expressed as combinations of the eigenmodes of the computational domain. This allows for an efficient numerical solution thanks to the use of Fast Fourier Transforms. The number of modes N_x controls the spatial discretization and the maximum simulated wavenumber is defined by $k_{\text{max}}^{\text{HOS}} = N_x\pi/L$ with L the length of the domain. The numerical environment includes a realistic wave maker and an absorbing zone at the end of the domain (set to prevent reflection from the opposite wall). HOS-NWT uses the same input as the experimental ECN facilities to describe the wave maker motion sequences. The model has been applied and validated for various configurations. This showed its accuracy and efficiency, see for instance (Suret et al., 2020; Ransley et al., 2021; Huchet et al., 2021; Kim et al., 2022; Xie et al., 2023).

[2] https://github.com/LHEEA/HOS-NWT

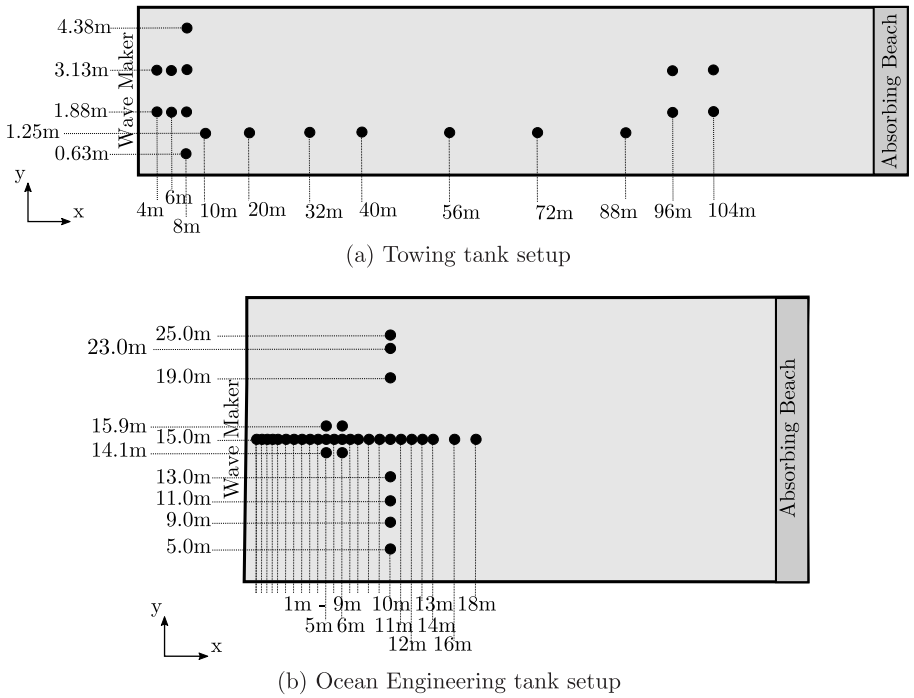

Fig. 2. Probe networks used for the experiments.

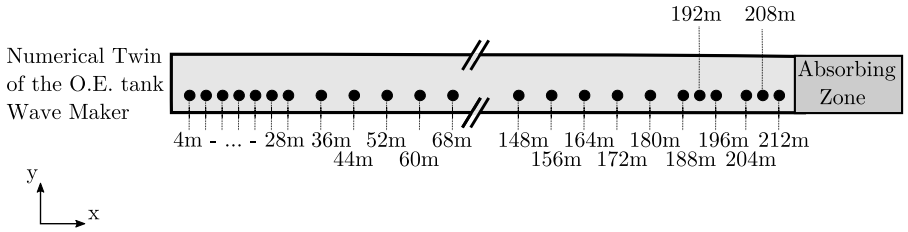

Fig. 3. Domain of the HOS-NWT simulations.

2.2.2. Numerical domain and set up

This digital twin enables some limitations associated with experiments, such as the length of the facility or the number of wave gauges, to be overcome. In this study, the numerical domain is an extended numerical version of the ECN O.E. tank. This enables the long-distance propagation that is required for the new wave generation procedure developed in this paper. The numerical wave maker mimics the O.E. tank wave maker (depth of 5 m and hinge 2.15 m from the bottom). The length is set at $L = 250$ m (instead of 50 m for the real O.E. tank). Numerical probes are placed all along the domain. Fig. 3 presents their position. Regarding the numerical set-up, the spatial discretization is set to $k_{\max}^{\mathrm{HOS}} = 25k_p$ and the order of nonlinearity is fixed to $M = 5$. This allows for an accurate nonlinear wave propagation. In addition, even if the generated wave conditions were non-breaking, the Tian-Barthelemy breaking model was implemented to prevent numerical instabilities for very steep waves. A description of this model can be found in Seiffert et al. (2017), Seiffert and Ducrozet (2018). Only one numerical breaking event every 500 waves or so was identified. This is not expected to influence the wave statistics studied. Note that the numerical setup and domain correspond to those of the study by Canard et al. (2022a). The reader is referred to the latter paper for more details.

In addition, in Section 5.1.2, numerical simulations twinning the Towing tank experiments are analyzed to better understand the experimental results. There, the domain geometry mimics the ECN Towing tank and the locations of the numerical probes follow the experimental set-up. $k_{\max}^{\mathrm{HOS}} = 25k_p$ and an order of nonlinearity of $M = 5$ are also adopted.

As for the experiments, for each numerical probe we used an analysis time window defined with Eqs. (1) and (2).

3. Nonlinear wave propagation in a water tank

In this section, we briefly present the spatial evolution of the statistics associated with a design sea state generated in a wave tank, to introduce the need to develop new wave generation methodologies to control the crest distribution at the target position X_t.

3.1. Wave condition

The design spectrum studied in this paper is the ss6g5 spectrum studied in Canard et al. (2022b,a). It is a non-breaking narrow-banded JONSWAP spectrum (see Komen et al. (1996)). Its shape is defined by

$$S(f) = \frac{\alpha_p g^2}{(2\pi)^4 f^5} \exp\left[-\frac{5}{4}\left(\frac{f}{f_p}\right)^{-4}\right] \gamma^{\exp[-(f-f_p)^2/(2s^2 f^2)]} \tag{4}$$

with $f_p = 1/T_p$ the peak frequency with T_p the peak period, α_p the Phillips parameter, γ the peak enhancement factor, and $s = 0.07$ for $f < f_p$ and $s = 0.09$ for $f > f_p$.

The spectrum parameters and the non-dimensional shape are provided in Table 1 and Fig. 4 respectively. See Appendix B for the definition of the mean period T_1, non-dimensional frequency bandwidth ν_w, and BFI. The spectrum (ss6g5) corresponds to a moderate design sea state (see NWT Preparation Workgroup (2019), Fouques

Table 1
Sea State Characteristics.

	Full scale	Scale 60	Scale 120
γ	5.0	5.0	5.0
H_s	6 m	0.10 m	0.05 m
T_p	12.25 s	1.60 s	1.12 s
T_1	10.63 s	1.37 s	0.97 s
λ_p	234 m	4 m	2 m
$k_p d$	12	12	12
$\epsilon_p = \frac{H_s}{\lambda_p}$	2.5%	2.5%	2.5%
ν_w	0.144	0.144	0.144
BFI	0.51	0.51	0.51

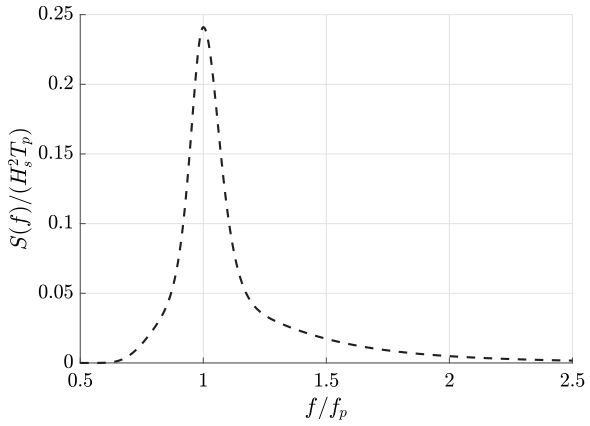

Fig. 4. ss6g5 design wave spectrum.

et al. (2021)) with a small ν_w, which is ensured by a significant $\gamma = 5$, representative of swell conditions (Det Norske Veritas, 2010). In this paper, ss6g5 was generated at scale 60 in the O.E tank and scale 120 in the Towing tank.

3.2. Spatial evolution of the wave spectrum

The data presented in this section were obtained after iteratively correcting the wave maker inputs to have the desired ss6g5 spectrum at the target location $X_t = 53\lambda_p$. At each iteration, a corrective coefficient is applied to the wave maker inputs in the Fourier space. It is computed as the ratio of the target amplitude to the measured one at X_t. The spectrum is considered as qualified if the relative error is below 10% around the peak frequency $f \in [0,75 f_p; 1,25 f_p]$. The correction is applied to the full frequency range covered by the wave maker (frequencies $f < 2$ Hz). Experimental limitations and uncertainties prevent the use of the qualification criteria in the low-energy frequency range. More details about this procedure can be found for instance in Canard et al. (2022b).

The ss6g5 sea state was generated experimentally at scale 120 in the ECN Towing tank. Four iterations were needed to obtain a qualified spectrum at $X_t = 53\lambda_p$. After correction, the dataset consisted of 30 realizations with a $395T_p$-duration (after the use of the analysis time windows). This wave field will be referred to as EXP ref $53\lambda_p$.

Complementary, a numerical ss6g5 wave field qualified at $X_t = 53\lambda_p$ was also generated. The data will be referred to as HOS ref $53\lambda_p$. As detailed in Section 2.2.2, the characteristics of the NWT relied on an extended 250-m-long version of the O.E. tank, and the generation scale was set to 60. Four corrective iterations on the wave-maker inputs were also needed to qualify the spectrum at X_t. The final dataset consisted of 35 realizations of duration $640T_p$. More details about the correction of the spectrum can be found in Canard et al. (2022b) for the experimental data and Canard et al. (2022a) for the numerical data.

The features of EXP ref $53\lambda_p$ and HOS ref $53\lambda_p$ are gathered in Table 2.

Table 2
Features of EXP ref $53\lambda_p$ and HOS ref $53\lambda_p$ datasets.

	EXP ref $53\lambda_p$	HOS ref $53\lambda_p$
Wave Tank	Experimental	Numerical
Domain	Towing Tank	Extended O.E. tank
Scale	120	60
Number of realizations	30	35
Total duration analyzed	$11{,}850T_p$	$22{,}400T_p$

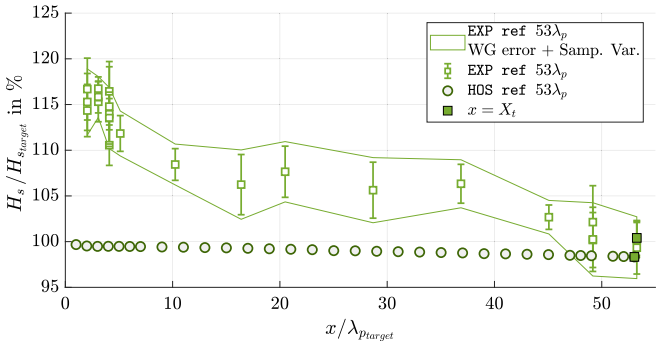

(a) H_s along the tank

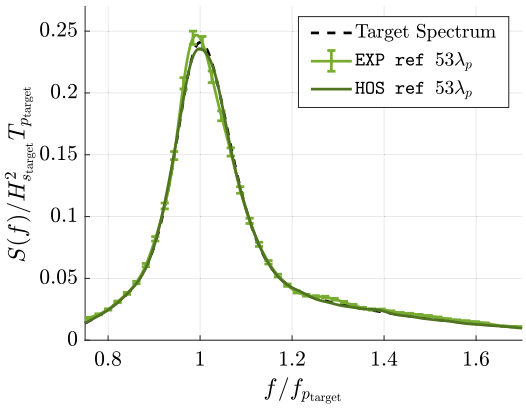

(b) Spectrum at $x = X_t$

Fig. 5. Spatial evolution of ss6g5 significant wave height (top) and wave spectrum at X_t (bottom).

Fig. 5(a) provides the spatial evolution of the significant wave height H_s and Fig. 5(b) displays the wave spectrum at the target location $S(f, x = X_t)$. From Fig. 5(a) it is clear that the experiments are affected by dissipation mechanisms (mostly due to side wall friction in this non-breaking sea state). This results in a H_s decrease along the tank. The correction of the spectrum adds energy at the beginning of the tank to balance this phenomenon at $x = X_t = 53\lambda_p$. As discussed in Canard et al. (2022b), the dissipation is likely to be induced by the side-wall friction. Note that at $x = 4\lambda_p$ the four probes settled at different transverse locations measured different H_s values. This suggests the presence of spurious transverse modes that limit the interpretation of the H_s evolution at the beginning of the tank. More discussion can be found in Canard et al. (2022b).

In contrast, the HOS-NWT model used to generate HOS ref $53\lambda_p$ does not include side-wall dissipation. This explains why H_s remains almost constant in the numerical simulations. The small amount of dissipation in the numerical simulations is attributed to the breaking model, which identified a few breaking events (one or two per realization). As expected from the correction procedure, at $x = X_t$, both HOS ref $53\lambda_p$ and EXP ref $53\lambda_p$ H_s reach $H_{s_{\text{target}}}$. Similarly, the spectra of both experimental and numerical data match ss6g5 target shape at the prescribed location X_t.

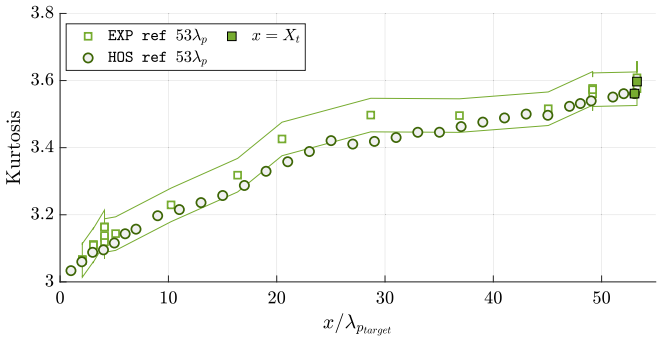

(a) Kurtosis along the tank

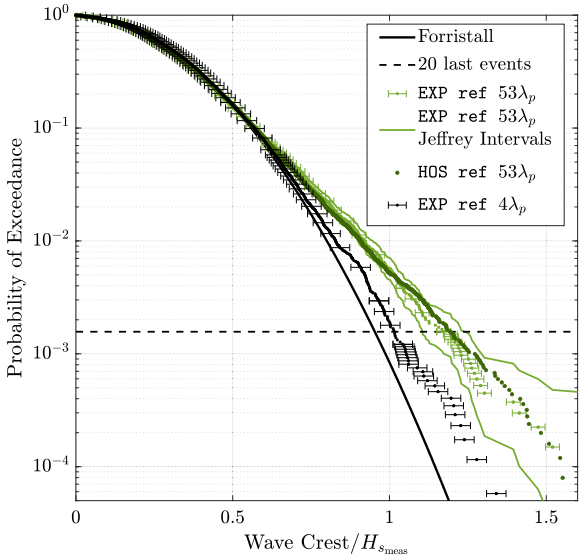

(b) Crest PDER at $x = X_t$

Fig. 6. Spatial evolution of ss6g5 statistics and crest distribution at X_t.

3.3. Spatial evolution of the wave statistics

Fig. 6(a) provides the spatial evolution of the kurtosis and Fig. 6(b) gives the crest Probability Distribution of the Ensemble of all the Realizations (PDER) at $x = X_t$, for both experimental and numerical wave tanks. The kurtosis is a scaled version of the fourth moment of the free surface elevation. It characterizes the tail of the free surface probability distribution and is widely used in ocean engineering to quantify with a simple parameter the severity of the wave field regarding extreme events (see for example (Kirezci et al., 2021; Annenkov and Shrira, 2009; Christou and Ewans, 2014)). For a linear wave field (Gaussian statistics), the kurtosis equals 3. This value increases when the probability of the extreme events is larger than the one predicted by the Gaussian distribution.

The different H_s behaviors observed in do not seem to significantly influence the spatial evolution of the extreme wave statistics. The spatial evolution of the kurtosis and the crest distribution at X_t remain highly similar between EXP ref 53λ_p and HOS ref 53λ_p datasets, see Fig. 6. It is important to note that different sets of random phases were used to generate the experimental and numerical wave fields. Therefore, the comparison between HOS ref 53λ_p and EXP ref 53λ_p is affected by sampling variability. Only the differences that fall outside the sampling-variability intervals (Jeffrey intervals for the crest distribution) can be considered indicative of a mismatch between the references, which is not the case here.

As expected for this unidirectional non-breaking moderate-BFI sea state, the kurtosis significantly increases along the tank. This is the result of high-order nonlinear phenomena such as near-resonant interactions and modulational instabilities (similar trends were observed for instance in Onorato et al. (2006), Fedele et al. (2010)). This means that the occurrence of extreme events increases with the distance from the wave maker. Concomitantly, the crest PDER at X_t exhibits a strong departure from the Forristall distribution for probabilities of exceedance below 5.10^{-3} (as a reminder, the Forristall reference accounts for the second-order nonlinear effects and is generally used as a reference in wave–structure interaction studies). See more details and interpretations of this behavior in Canard et al. (2022b).

To emphasize the influence of the target location, we also plotted in Fig. 6(b) the distribution obtained at $X_t = 4\lambda_p$, after correction of the spectrum at this location in the Towing tank. Note that this dataset differs from EXP ref 53λ_p, and will be referred to as EXP ref 4λ_p. EXP ref 53λ_p and EXP ref 4λ_p wave fields exhibit the exact same spectrum at their respective target locations. However, we observe a strong difference between the two distributions. The occurrence of the extreme events is significantly larger at $X_t = 53\lambda_p$. The distribution of EXP ref 4λ_p is far less extreme and is closer to the Forristall reference (even if a small departure is already observed). The detailed comparison of these two datasets can be found in Canard et al. (2022b).

This means that qualifying the spectrum at a given target distance X_t is not enough to control the crest distribution at this location. When generating wave fields for wave–structure interaction studies, such different statistical behaviors can lead to significantly different responses of the structure. A first step towards more relevant wave generation and qualification methods is therefore to control the wave statistics generated at a given target distance from the wave maker. This is the objective of the wave generation procedure introduced in the next section and tested in the rest of this paper.

4. Wave generation procedure with controlled statistics

The environmental conditions for a wave–structure interaction study are determined by several features such as the typology of the structure, the location, and the classification society rule that needs to be fulfilled. For each case, a list of wave spectra to be tested is defined (the so-called design spectra). The requirements of classification societies are usually limited to the specification of the spectrum shape, together with a probability (or equivalently a test duration). However, this does not characterize completely the wave statistics as discussed in Section 3.3. For now, there is no prescription of the crest distribution or kurtosis value to target. Most of the crest distributions observed in situ roughly follow the weakly non-linear Forristall or Tayfun references (Forristall, 2000; Tayfun and Fedele, 2007; Häfner et al., 2021). However, it has also been found that extreme distributions can occur for unstable conditions (young sea states (Toffoli et al., 2024), wind speed or direction change (Annenkov and Shrira, 2009), bathymetry change (Ducrozet and Gouin, 2017), or spatially varying current (Ducrozet et al., 2021)).

The methodology introduced in this section has been developed to take account of this statistical variability, by giving the possibility of targeting a prescribed crest distribution (or kurtosis value) in addition to the design spectrum (when the state-of-the-art procedures only allow the generation of the design spectrum).

4.1. Definition of X_t and $X_{t_{\text{stat}}}$

We consider a wave–structure interaction study with a prescribed target spectrum and crest distribution (or kurtosis value). The first step is to define the experimental setup (wave tank, model scale, mooring arrangement, etc.). This determines the model position in the wave tank, which will be the target position X_t. Next, the experimenter must generate the sea state and measure the waves throughout the tank without the model. Note that this step can be carried out in a numerical twin of the tank, which allows the use of an extended (longer) domain. These initial results are used to identify the location at which the

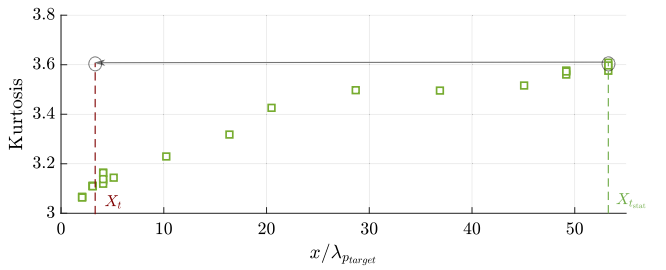

(a) Bringing the design sea state closer to the wave maker: $X_{t_{\text{stat}}} > X_t$

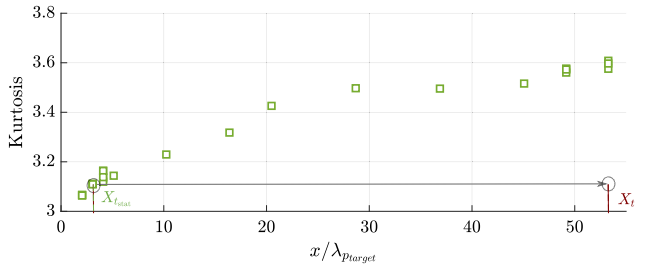

(b) Moving the design sea state away from the wave maker: $X_{t_{\text{stat}}} < X_t$

Fig. 7. Illustration of the objectives of the new procedure, using the spatial evolution of the EXP `ref` $53\lambda_p$ `kurtosis`.

crest distribution/kurtosis reaches the target one. This position will be referred to as $X_{t_{\text{stat}}}$.

The objective of the newly introduce procedure is then to generate at the target location X_t: (i) the qualified target wave spectrum and (ii) the target crest distribution/kurtosis that is usually associated with the location $X_{t_{\text{stat}}}$, when using the state-of-the-art generation procedures.

This objective is illustrated in Fig. 7 using the curve of the kurtosis evolution along the tank. As observed in the previous section, due to the spatial evolution of the statistics (induced mainly by modulational instabilities), a large probability of extreme events (kurtosis values far larger than 3, strong departure of the tail of the crest distributions) is associated with large values of $X_{t_{\text{stat}}}$, and kurtosis values closer to 3 and crest distributions that are close to the second order references (such as the Forristall one (Forristall, 2000)) are associated with small values of $X_{t_{\text{stat}}}$.

We present here a wave generation procedure that works for $X_{t_{\text{stat}}} > X_t$ (generation closer to the wave maker of the extreme distributions that usually appear further in the tank, see Fig. 7(a)) and $X_{t_{\text{stat}}} < X_t$ (generation further in the tank of the non-extreme distributions that usually appear closer to the wave maker, see Fig. 7(b)).

4.2. Bringing extreme wave statistics closer to the wave maker: $X_{t_{\text{stat}}} > X_t$

Fig. 8 presents the proposed procedure for $X_{t_{\text{stat}}} > X_t$, which allows for generating sea states with extreme statistics closer to the wave maker. It can be decomposed into two steps. First, the design spectrum is generated at $x = X_{t_{\text{stat}}}$, by iterating on the wave-maker inputs to ensure its quality, see *e.g.* (Canard et al., 2022a). Following the qualification procedure proposed in Fouques et al. (2021), this correction ensures that the relative spectrum error at $X_{t_{\text{stat}}}$ is below 10% for f in the range $[0.75f_p; 1.25f_p]$. At the end of this first step, we have a wave field of N_{run} realizations that exhibit at $x = X_{t_{\text{stat}}}$: (i) the target design spectrum $S_{\text{design}}(f)$ and (ii) the wave statistics associated with the nonlinear propagation up to $X_{t_{\text{stat}}}$, considered as the target ones. Note that the waves need to be measured at least at $x = X_{t_{\text{stat}}}$ and $x = X_{t_{\text{stat}}} - X_t$ (respectively green and gray locations in Fig. 8).

Then, the second step of the procedure uses the waves measured at $x = X_{t_{\text{stat}}} - X_t$ to create input sequences for a second generation in the wave tank. The new wave maker motion consequently uses as input: $\eta^{\text{step2}}_{\text{input}}(t) = \eta^{\text{step1}}(t, X_{t_{\text{stat}}} - X_t)$. The use of recorded wave signals in wave maker motion is a well-known and controlled process, used for instance to artificially increase the length of an experimental wave tank (see *e.g.* (Chabchoub et al., 2012)). For the present procedure, the idea is to reproduce between the wave maker (located at $x = 0$) and $x = X_t$, the wave propagation that occurred at Step 1 between $X_{t_{\text{stat}}} - X_t$ and $X_{t_{\text{stat}}}$. It is important to note that to build the wave maker motion we use the Fourier transforms of $\eta^{\text{step2}}_{\text{input}}(t)$ sequences. The nonlinear wave signals are converted into a linear sum of Fourier components. As a consequence, the measured bound waves are converted into free waves by the wave maker. This is a source of uncertainty in the current procedure that could be removed using different strategies if needed. However, it has not been seen as necessary regarding the results presented in Section 5.

At the end of Step 2, the wave field at $x = X_t$ (red position in Fig. 8) should exhibit: (i) the design spectrum (qualified $S(f, X_t) = S_{\text{design}}(f)$) and (ii) the wave statistics naturally emerging at $X_{t_{\text{stat}}}$.

4.3. Moving the non-extreme wave statistics away from the wave maker: $X_{t_{\text{stat}}} < X_t$

To complement the previous subsection, the present one focuses on the case where one wants to impose far from the wave maker, the wave statistics that usually occur closer, i.e. $X_{t_{\text{stat}}} < X_t$. In this configuration, the previous procedure is modified and includes the concept of Time-Reversal (TR) mirrors (Fink, 1992). The latter makes use of the time reversibility of the wave propagation in a conservative medium to reconstruct the past evolution of wave dynamics. The method has been used in various contexts: acoustics, optics, and water waves (Fouque and Nachbin, 2003; Chabchoub and Fink, 2014).

Practically, the methodology involves two steps for the wave propagation in an experimental or numerical tank. First, a given target wave sequence $\eta^{\text{step1}}_{\text{input}}(t)$ is sent as input to the wave maker at $x = 0$. The resulting wave field is measured at a distance $x = x_{\text{meas}}$. Then, the measurements at $x = x_{\text{meas}}$, $\eta(t, x_{\text{meas}})$ with $t \in [0; t_{\text{end}}]$, are mirrored in time, and sent as an input to the wave generator: $\eta^{\text{step2}}_{\text{input}}(t) = \eta(t_{\text{end}} - t, x_{\text{meas}})$

If the wave propagation is conservative (no dissipation, no breaking events), the waves measured during the second experiment at $x = x_{\text{meas}}$ correspond to the exact initial input wave sequence mirrored in time $\eta^{\text{step2}}(t, x_{\text{meas}}) = \eta^{\text{step1}}_{\text{input}}(t_{\text{end}} - t)$. This allows for accurately moving target wave profiles away from the wave maker. For instance, the method was successfully used in Ducrozet et al. (2020) to generate different rogue wave profiles at specific locations in a wave tank.

Combining the TR methodology with the previous procedure to control wave statistics, we propose a second procedure to reproduce at a position of interest X_t the sea state and the associated wave statistics that initially occurred at $X_{t_{\text{stat}}} < X_t$.

The procedure is illustrated in Fig. 9. As for the $X_{t_{\text{stat}}} > X_t$ case, in Step 1 the design spectrum is first accurately generated at $x = X_{t_{\text{stat}}}$ (green position in Fig. 9), iterating on the wave maker inputs. During this first step, the waves are measured at $x_{\text{meas}} = X_{t_{\text{stat}}} + X_t$ (gray position in Fig. 9). Then, these recorded waves are mirrored in time and sent to the wave maker for the second step:

$$\eta^{\text{step2}}_{\text{input}}(t) = \eta^{\text{step1}}(t_{\text{end}} - t, X_{t_{\text{stat}}} + X_t) \tag{5}$$

The idea is to reproduce, between the wave maker and X_t, the space-and-time mirrored wave propagation that occurred at Step 1 between $X_{t_{\text{stat}}}$ and $X_{t_{\text{stat}}} + X_t$. At the end of Step 2, the wave field at X_t (red position in Fig. 9) should exhibit: (i) the design spectrum (qualified $S(f, X_t) = S_{\text{design}}(f)$) and (ii) the wave statistics naturally emerging at $X_{t_{\text{stat}}}$.

The time-reversal methodology does not work when dissipation occurs. Consequently, the procedure for $X_{t_{\text{stat}}} < X_t$ cannot be applied in its current state in the ECN Towing tank where sidewall dissipation is significant (see). Only a numerical validation will be provided in this paper for $X_{t_{\text{stat}}} < X_t$.

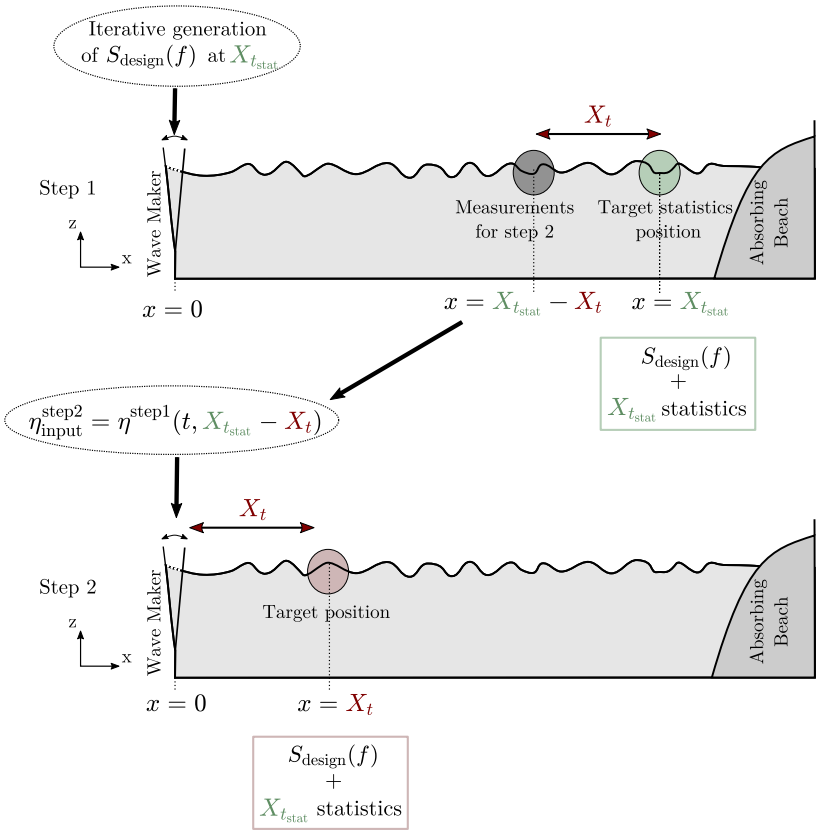

Fig. 8. Procedure to generate a qualified wave field with controlled statistics, for $X_{t_{\text{stat}}} > X_t$.

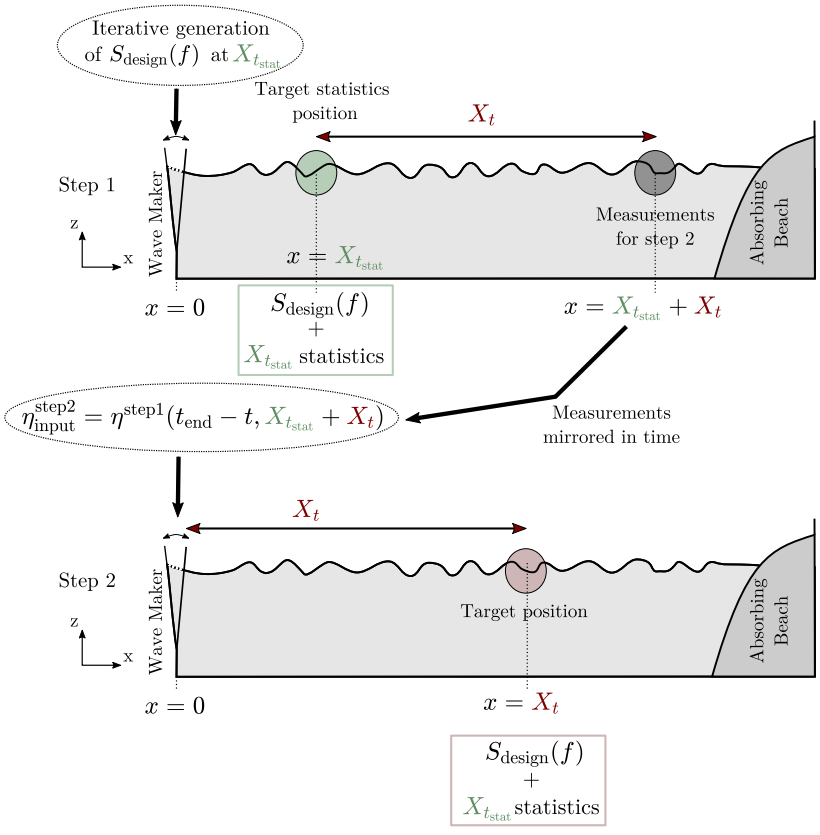

Fig. 9. Procedure to generate a qualified wave field with controlled statistics, for $X_{t_{\text{stat}}} < X_t$.

Table 3
Generated Wave fields and naming convention.

	Domain	X_t	$X_{t_{stat}}$
EXP ref $53\lambda_p$	T. tank	$53\lambda_p$	/
EXP ref $53\lambda_p$ reprod $4\lambda_p$	T. tank & num. T. tank	$4\lambda_p$	$53\lambda_p$
HOS ref $53\lambda_p$	Extended num. O.E. tank	$53\lambda_p$	/
HOS ref $53\lambda_p$ reprod $4\lambda_p$	Extended num. O.E. tank & O.E. tank	$4\lambda_p$	$53\lambda_p$
HOS ref $4\lambda_p$	Extended num. O.E. tank	$4\lambda_p$	/
HOS ref $4\lambda_p$ reprod $53\lambda_p$	Extended num. O.E. tank	$53\lambda_p$	$4\lambda_p$

For both $X_{t_{stat}} > X_t$ and $X_{t_{stat}} < X_t$ cases, the procedure provides for Step 2 input wave sequences adapted to X_t and $X_{t_{stat}}$, based on a spectral shape different from that of the input target spectrum and non-random phases. It can be used numerically and experimentally. Hybrid approaches using a numerical solver to carry out Step 1 to directly generate Step 2 in an experimental tank should also be considered to save experimental time. Furthermore, for the $X_{t_{stat}} > X_t$ case, as the numerical domain can be extended as desired, carrying out step 1 numerically makes it possible to access large $X_{t_{stat}}$ values that are not always available as experimental tanks have a limited size.

5. Results and discussion

The remainder of this paper is now devoted to the numerical and experimental validation of the two procedures described in Figs. 8 and 9. It is important to emphasize that the following results are based on wave studies only (there are no structures in the domain).

First, the procedure will be tested to reproduce the extreme EXP ref $53\lambda_p$ and HOS ref $53\lambda_p$ (studied in Section 3) wave fields of the ss6g5 sea state measured at $x = 53\lambda_p$, closer to the wave maker, at $x = 4\lambda_p$. This means that $X_t = 4\lambda_p$ and $X_{t_{stat}} = 53\lambda_p$. In other words, the objective is to generate at $X_t = 4\lambda_p$: (i) the qualified ss6g5 spectrum, and (ii) the extreme distributions that were only observed at $X_{t_{stat}} = 53\lambda_p$ (see Fig. 6(b)).

Then, the procedure for $X_{t_{stat}} < X_t$ will be tested numerically using the HOS-NWT domain described in Section 2.2.2, again for the ss6g5 sea state, but with $X_{t_{stat}} = 4\lambda_p$ and $X_t = 53\lambda_p$. This time, the objective will be to move the non-extreme wave statistics associated with $x = 4\lambda_p$ away from the wave maker.

The wave field data, recorded at the end of the second step of both procedures at $x = X_t$ will be compared to the waves measured at $x = X_{t_{stat}}$ at the end of Step 1. Note that for each comparison, the analysis time windows and the sets of realizations are meticulously chosen to ensure that the same wave sequences are being compared. No sampling variability affects the comparisons.

Table 3 lists the generated cases that will be studied throughout this section.

5.1. Reproduction of the $X_{t_{stat}} = 53\lambda_p$ experimental reference at $X_t = 4\lambda_p$

We focus first on the reproduction at $x = X_t = 4\lambda_p$ of the EXP ref $53\lambda_p$ waves measured at $x = X_{t_{stat}} = 53\lambda_p$, using the newly introduced procedure. In the following, this reproduction will be labeled as EXP ref $53\lambda_p$ reprod $4\lambda_p$.

5.1.1. Full experimental procedure

The different realizations of EXP ref $53\lambda_p$ reprod $4\lambda_p$ were first run experimentally in the Towing tank.

Deterministic reproduction. Fig. 10 presents a comparison in the time domain between EXP ref $53\lambda_p$ at $X_{t_{stat}}$ and EXP ref $53\lambda_p$ reprod $4\lambda_p$ at X_t, for a duration of 60 peak periods. No significant differences are observed when changing the time window. The EXP ref $53\lambda_p$ reprod $4\lambda_p$ measurements align with the EXP ref $53\lambda_p$ data. The slight discrepancies between the two signals arise from: (i) the linear conversion of EXP ref $53\lambda_p$ measured wave signals into EXP ref $53\lambda_p$ reprod $4\lambda_p$ wave maker input sequences, and (ii) the control of the Towing tank wave maker motions.

Reproduction of the spectrum. Fig. 11 presents a comparison of different stochastic quantities. Panel 11(a) presents the spatial evolution of the significant wave height H_s. We observe a small discrepancy in the wave maker transfer function. This results in an overshoot of 3 to 4 percent for EXP ref $53\lambda_p$ reprod $4\lambda_p$ (red curve) near the wave maker. This is also visible in the time domain comparison in Fig. 10, where the red curve draws slightly greater heights. Consequently, the EXP ref $53\lambda_p$ reprod $4\lambda_p$ spectrum at X_t is not qualified. It contains excessive energy, particularly around its peak and near $f = 1.3f_{p_{target}}$ (see panel 11(b))

To overcome this issue, the iterative spectrum correction procedure was applied to adjust EXP ref $53\lambda_p$ reprod $4\lambda_p$ inputs to balance the behavior of the Towing tank wave maker. Note that the correction slightly adjusts the input amplitudes, but does not modify the phases. The resulting wave field corresponds to the orange curves in Fig. 11. The excess energy overshoot has been successfully rectified. The spectrum at X_t aligns with the ss6g5 target shape, within the wave gauges' uncertainty ranges. And the significant wave height reaches 99.3% of $H_{s_{target}}$ at X_t. The first objective is reached, and with an additional correction, the spectrum is qualified at $X_t = 4\lambda_{p_{target}}$.

Reproduction of the kurtosis and crest distribution. Fig. 11(c) presents the spatial evolution of the kurtosis along the tank. As expected, for EXP ref $53\lambda_p$ reprod $4\lambda_p$, the wave maker directly generates the extreme wave field that occurs at the end of the tank for EXP ref $53\lambda_p$. Consequently, EXP ref $53\lambda_p$ reprod $4\lambda_p$ kurtosis at $x = X_t = 4\lambda_{p_{target}}$ equals 3.40, instead of the 3 to 3.1 values observed at this location when using standard wave generation procedures. The 3.52 value obtained for EXP ref $53\lambda_p$ at $x = X_{t_{stat}}$ is almost reached. The remaining difference arises due to a combination of factors including wave maker defects, experimental uncertainties, and the conversion of $X_{t_{stat}} - X_t$ EXP ref $53\lambda_p$ signals into wave maker inputs. A more detailed investigation will be conducted in the upcoming subsection, based on numerical simulations. However, the effects remain limited, and a strong departure from Gaussianity is observed from the beginning of the tank thanks to the proposed procedure. No significant change in kurtosis is observed between the raw reproduction (red curve) and the reproduction after correcting the spectrum (orange curve). The spatial dynamics of the wave statistics are mainly controlled by the phases of the wave components generated by the wave maker.

Fig. 11(d) displays the EXP ref $53\lambda_p$ reprod $4\lambda_p$ crest PDER obtained at $x = X_t = 4\lambda_p$. It nearly reaches the EXP ref $53\lambda_p$ extreme distribution measured at $x = X_{t_{stat}}$. As observed in the analysis of kurtosis, the probability of extreme events for EXP ref $53\lambda_p$ reprod $4\lambda_p$ is slightly smaller. This difference becomes significantly more pronounced for probabilities below 2.10^{-3}. However, the distribution is undoubtedly extreme and significantly larger than the usual PDER obtained at $4\lambda_p$, EXP ref $4\lambda_p$, drawn in black in Fig. 11(d). Note that the additional spectrum correction of EXP ref $53\lambda_p$ reprod $4\lambda_p$ does not affect the kurtosis and the crest PDER.

5.1.2. Limitations due to the Towing tank wave maker

To investigate the remaining discrepancies between the crest distributions of EXP ref $53\lambda_p$ reprod $4\lambda_p$ at X_t and EXP ref $53\lambda_p$ at $X_{t_{stat}}$, HOS-NWT simulations were conducted, reproducing the Towing tank EXP ref $53\lambda_p$ reprod $4\lambda_p$ experiments. For these specific simulations, the HOS-NWT domain mimicked the geometry of the Towing tank.

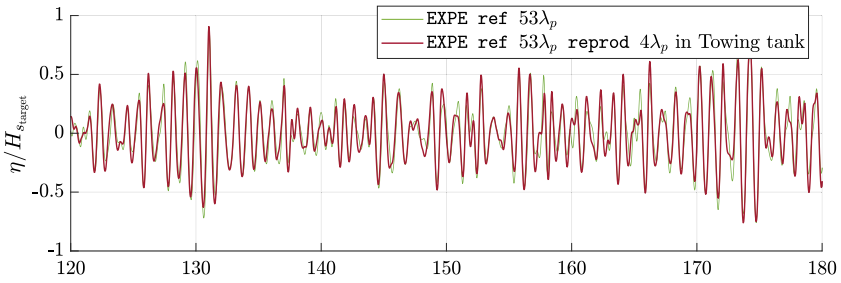

Fig. 10. Time-domain comparison of EXP ref $53\lambda_p$ at $X_{t_{stat}}$ and EXP ref $53\lambda_p$ reprod $4\lambda_p$ at X_t.

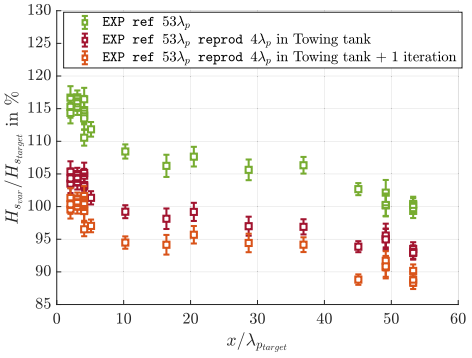

(a) H_s along the tank

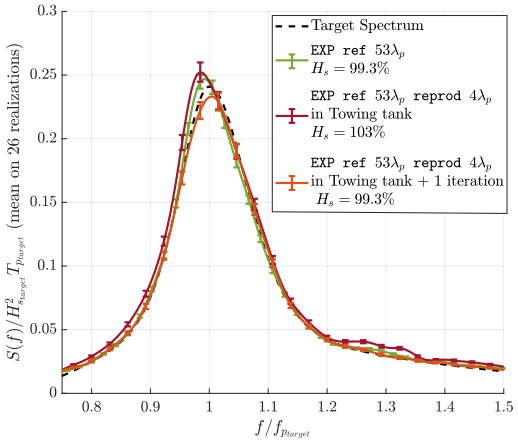

(b) EXP ref $53\lambda_p$ reprod $4\lambda_p$ spectrum at X_t versus EXP ref $53\lambda_p$ at $X_{t_{\text{stat}}}$

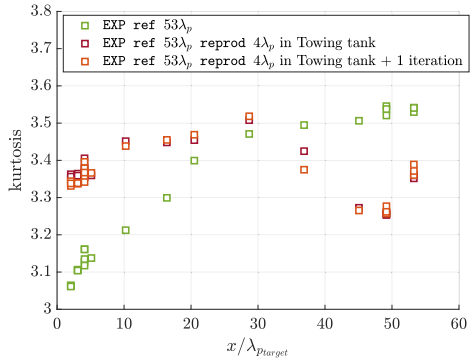

(c) kurtosis along the tank

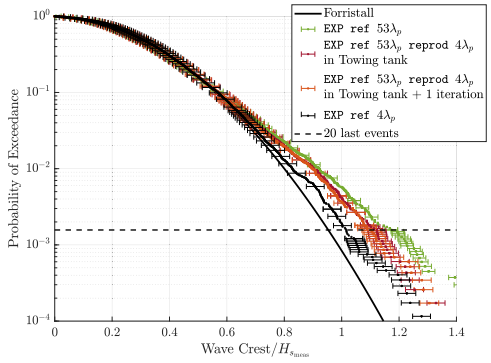

(d) EXP ref $53\lambda_p$ reprod $4\lambda_p$ crest PDER at X_t versus EXP ref $53\lambda_p$ at $X_{t_{\text{stat}}}$

Fig. 11. Comparison of EXP ref $53\lambda_p$ and EXP ref $53\lambda_p$ reprod $4\lambda_p$ generated in the Towing tank.

Two sets of simulations were run: (i) one referred to as "EXP ref $53\lambda_p$ reprod $4\lambda_p$ in HOS," which used the EXP ref $53\lambda_p$ reprod $4\lambda_p$ input sequences, and (ii) one labeled as "EXP ref $53\lambda_p$ reprod $4\lambda_p$ in HOS with measured Exp. WVMK" which used the recorded wave maker motions from the Towing tank experiments as inputs. The aim was to assess the impact of potential discrepancies between the input motions and the actual motions recorded during the EXP ref $53\lambda_p$ reprod $4\lambda_p$ experiments.

Fig. 12 presents the results. For the sake of readability, uncertainty bars were removed from the experimental spectra and crest distributions (panels 12(b) and 12(d)). First, we can see in panel 12(a) that the significant wave height of the two HOS-NWT datasets remains constant along the tank, as no dissipation model has been implemented to account for side-wall friction, which affects the experimental results. Apart from this discrepancy, EXP ref $53\lambda_p$ reprod $4\lambda_p$ in HOS with measured Exp. WVMK accurately reproduces the experiments. The kurtosis, spectrum, and crest distribution are also nearly identical when using as input the measured wave maker motion. Additionally, the same significant wave height overshoot observed in the experimental data is reproduced in the HOS-NWT results.

In contrast, when using the EXP ref $53\lambda_p$ reprod $4\lambda_p$ input sequences directly, the overshooting of significant wave height disappears, and the kurtosis increases slightly. This suggests that the energy overshoot and the slight reduction in the height of extreme events observed in the experimental data come from discrepancies between the imposed wave maker motion sequences and the target ones. However, the crest distribution of EXP ref $53\lambda_p$ reprod $4\lambda_p$ in HOS at X_t does not show a significant improvement and still does not

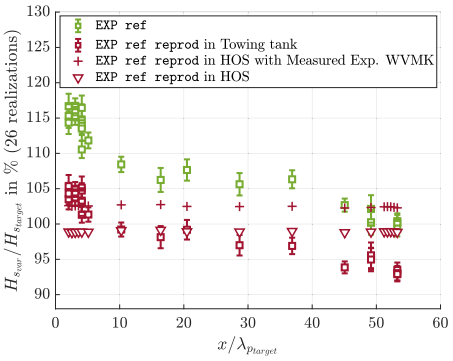

(a) H_s along the tank

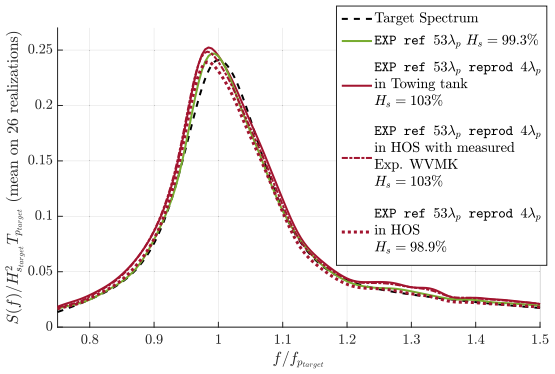

(b) EXP ref $53\lambda_p$ reprod $4\lambda_p$ spectrum at X_t versus EXP ref $53\lambda_p$ at $X_{t_{\text{stat}}}$

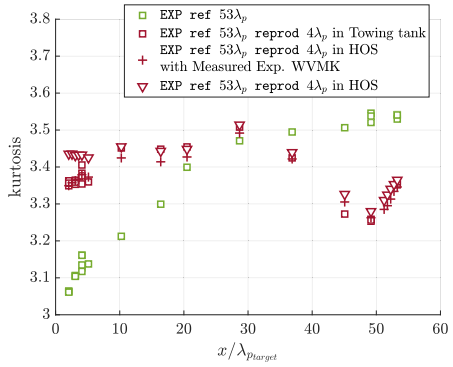

(c) kurtosis along the tank

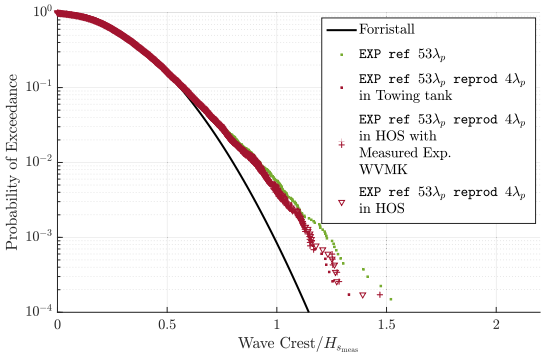

(d) EXP ref $53\lambda_p$ reprod $4\lambda_p$ crest PDER at X_t versus EXP ref $53\lambda_p$ at $X_{t_{\text{stat}}}$

Fig. 12. Influence of the Towing tank wave maker defects on EXP ref $53\lambda_p$ reprod $4\lambda_p$ statistics at X_t.

reach the EXP ref $53\lambda_p$ reference measured at $X_{t_{\text{stat}}}$. The remaining errors most likely come from the experimental uncertainties and the conversion of $X_{t_{\text{stat}}} - X_t$ EXP ref $53\lambda_p$ signals into wave maker inputs.

5.1.3. Conclusion

The study gives an example of a fully experimental application of the procedure. Even if the accuracy of the EXP ref $53\lambda_p$ reprod $4\lambda_p$ waves is somewhat restricted due to experimental constraints, the objectives are reached. Both a qualified spectrum and an extreme distribution, relying approximately on the $X_{t_{\text{stat}}} = 53\lambda_{p_{\text{target}}}$ reference, were generated at $X_t = 4\lambda_{p_{\text{target}}}$. The remaining error only affects the height of the most extreme events which are very sensitive and occur at probabilities below the typical probabilities used for design.

5.2. Experimental and numerical reproduction of the numerical reference: validation of the hybrid approach

It is important to state that conducting the complete procedure experimentally (as done in the previous subsection) poses significant challenges. First, it requires large-duration experiments. For instance, the generation of EXP ref $53\lambda_p$ required four iterations, each consisting of at least five 15-min runs. Then, 30 realizations of the qualified wave field were generated. Lastly, the second step also demands 30 additional realizations. This results in a combined total of 80 realizations, equivalent to a minimum of one week of experiments. Moreover, when targeting extreme wave statistics, the $X_{t_{\text{stat}}}$ value is large and the first step of the procedure requires a long wave tank. This limits the application of the procedure to long wave channels that are usually not available for ocean engineering experiments.

To tackle those issues, a viable solution is to use a numerical wave propagation solver such as HOS-NWT to generate the qualified spectrum at $X_{t_{\text{stat}}}$. This significantly decreases the duration of the study compared to experimental campaigns. Then the second step of the procedure (i.e. the generation of the reference wave field at X_t) can be conducted either experimentally in any wave tank (the domain does not need to include $X_{t_{\text{stat}}}$) or numerically, for instance to build wave conditions for CFD wave–structure interaction studies.

This hybrid approach is tested in the present subsection, in which we address a new practical case, the reproduction of the numerical reference HOS ref $53\lambda_p$ waves, occurring at $X_{t_{\text{stat}}} = 53\lambda_{p_{\text{target}}}$, closer to the wave maker at $X_t = 4\lambda_p$. The resulting wave fields are denoted as HOS ref $53\lambda_p$ reprod $4\lambda_p$ for which different realizations were conducted both experimentally in the Ocean Engineering tank, and numerically using HOS-NWT within the same numerical wave tank used for running HOS ref $53\lambda_p$ (see Section 2.2.2).

Fig. 13 presents the results. The O.E. tank's length of 50 m and the positioning of the probe network confine the experimental data within $x \in [0, 5]\lambda_p$. As a reminder, the HOS-NWT domain used for conducting the numerical simulation is an extension of the O.E. tank, elongated to 250 m, to encompass $X_{t_{\text{stat}}} = 53\lambda_p = 208$ m.

For both the numerical and experimental versions of HOS ref $53\lambda_p$ reprod $4\lambda_p$ the procedure works well. At $x = X_t = 4\lambda_p$, the ss6g5 H_s (panel 13(a)) and qualified target spectrum shape (panel 13(b)) are generated. Moreover, the extreme HOS ref $53\lambda_p$ distribution occurring at $X_{t_{\text{stat}}} = 53\lambda_p$ is also accurately reproduced (panel 13(d)). The black curve shows the experimental reference distribution obtained for $X_t = 4\lambda_p$ when using the state-of-the-art generation procedure. Using the new procedure we were able to generate, both numerically

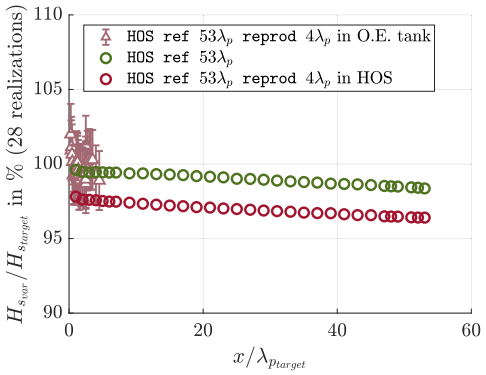

(a) H_s along the tank

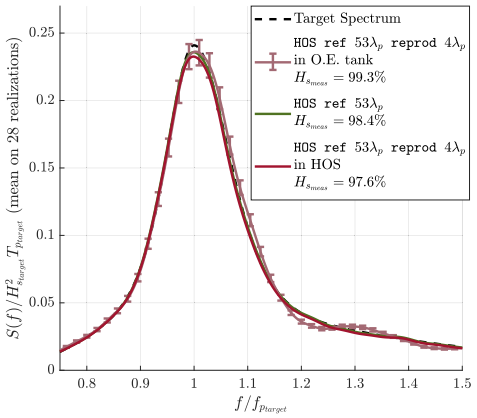

(b) `HOS ref` $53\lambda_p$ `reprod` $4\lambda_p$ spectrum at X_t versus `HOS ref` $53\lambda_p$ at $X_{t_{\text{stat}}}$

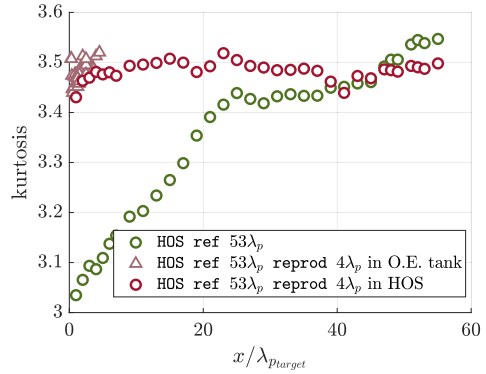

(c) kurtosis along the tank

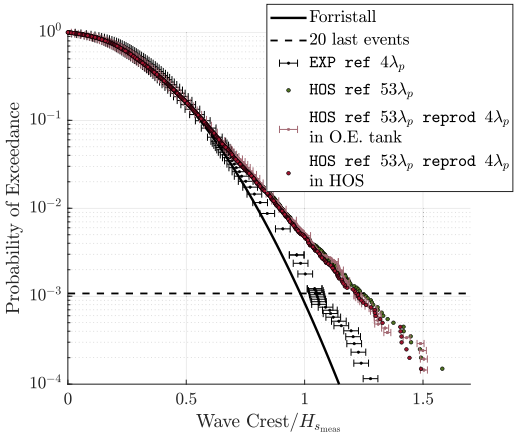

(d) `HOS ref` $53\lambda_p$ `reprod` $4\lambda_p$ crest PDER at X_t versus `HOS ref` $53\lambda_p$ at $X_{t_{\text{stat}}}$

Fig. 13. Comparison of `HOS ref` $53\lambda_p$ and `HOS ref` $53\lambda_p$ `reprod` $4\lambda_p$ generated with `HOS-NWT` and in the O.E. tank.

and experimentally, a far more extreme crest distribution at this same target location $X_t = 4\lambda_p$.

Unlike the case of `EXP ref` $53\lambda_p$ `reprod` $4\lambda_p$, no additional spectrum correction was needed and the O.E. tank wave maker perfectly reproduced the statistics. Both the fully numerical and the hybrid approaches (involving the generation of the $X_{t_{\text{stat}}}$ reference with `HOS-NWT` and its reproduction at X_t using experimental facilities) are successfully validated.

5.3. Test of the procedure for $X_{t_{\text{stat}}} < X_t$: moving away moderate statistics from $X_{t_{\text{stat}}} = 4\lambda_p$ to $X_t = 53\lambda_p$

We now address the validation of the procedure for the control of wave statistics in a configuration where $X_{t_{\text{stat}}} < X_t$. As a reminder, the methodology includes the use of the TR methodology (see Section 4.3 and Fig. 9). This means that the procedure, in its current state, does not work when dissipation occurs (as is the case in the ECN Towing tank). Therefore, we only address here the numerical validation of the procedure.

Contrary to the previous subsection, the objective is now to produce a sea state exhibiting mild extreme statistics far from the wave maker. We tested the procedure with $X_{t_{\text{stat}}} = 4\lambda_p$ and $X_t = 53\lambda_p$. We first generated a qualified `ss6g5` design spectrum at $X_{t_{\text{stat}}} = 4\lambda_p$ (position associated with wave statistics of moderate severity) in the `HOS-NWT` domain. Then, this wave field was reproduced further in the tank, at $X_t = 53\lambda_p$ (position associated with extreme statistics with the state-of-the-art procedures), by using as input the measured waves at $X_{t_{\text{stat}}} + X_t = 57\lambda_p$, mirrored in time (a numerical probe was placed at the latter position). The wave field obtained at the end of the first step, whose spectrum is the qualified spectrum at $x = X_{t_{\text{stat}}} = 4\lambda_p$ will be referred to as `HOS ref` $4\lambda_p$. Its reproduction at $x = X_t = 53\lambda_p$ (second step of the procedure) will be referred to as `HOS ref` $4\lambda_p$ `reprod` $53\lambda_p$.

First, Fig. 14 compares in the time domain `HOS ref` $4\lambda_p$ measurements at $X_{t_{\text{stat}}} = 4\lambda_p$ and `HOS ref` $4\lambda_p$ `reprod` $53\lambda_p$ measurements at $X_t = 53\lambda_p$ mirrored in time. The plotted time window lasts for $60T_p$ and was chosen randomly as results were similar for the whole duration.

If the procedure had worked perfectly, the two free surface elevation time series would have been identical. What we observe here is that the main patterns are recovered but noticeable discrepancies remain. The quality of the wave field reproduction in the time domain is lower than what was observed for the $X_{t_{\text{stat}}} > X_t$ case studied in the previous subsection, see Fig. 10. It is important to note that we used here the time reversal technique to reproduce long-duration realizations, whereas the method has mainly been validated to reproduce individual events (Ducrozet et al., 2020). The discrepancies can be due to the linear conversion of the nonlinear measurements at $X_{t_{\text{stat}}} + X_t$ mirrored in time, into a linear sum of free-wave components in the Fourier space sent as input to the wave maker. More generally, the propagating distance mirrored in space and time was large: $53\lambda_p$. Hence, small errors in the construction or generation of the input wave field can lead to larger discrepancies at $X_t = 53\lambda_p$.

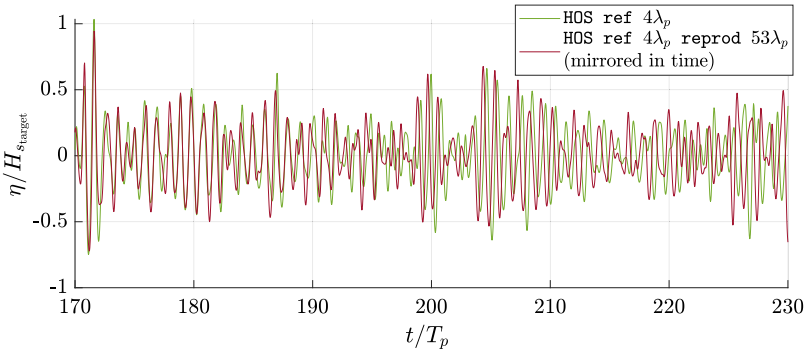

Fig. 14. Time-domain comparison of HOS ref $4\lambda_p$ measurements at $X_{t_{stat}} = 4\lambda_p$ and HOS ref $4\lambda_p$ reprod $53\lambda_p$ measurements at $X_t = 53\lambda_p$ mirrored in time.

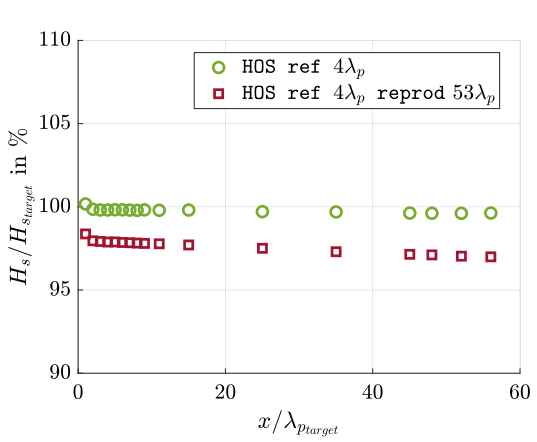

(a) H_s along the tank

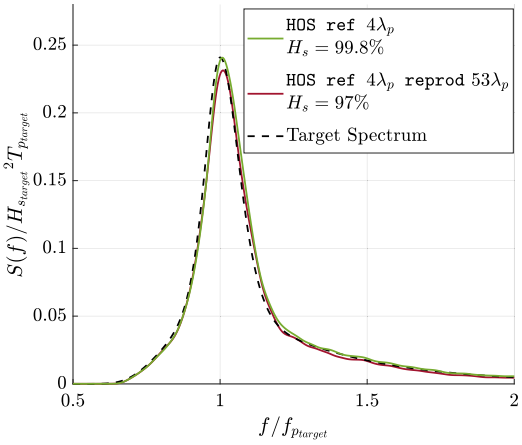

(b) HOS ref $4\lambda_p$ reprod $53\lambda_p$ spectrum at X_t versus HOS ref $4\lambda_p$ at $X_{t_{\text{stat}}}$

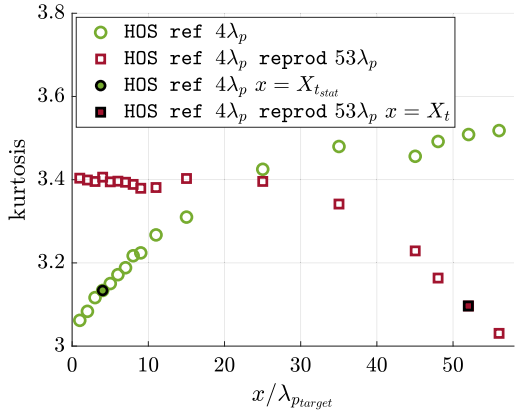

(c) kurtosis along the tank

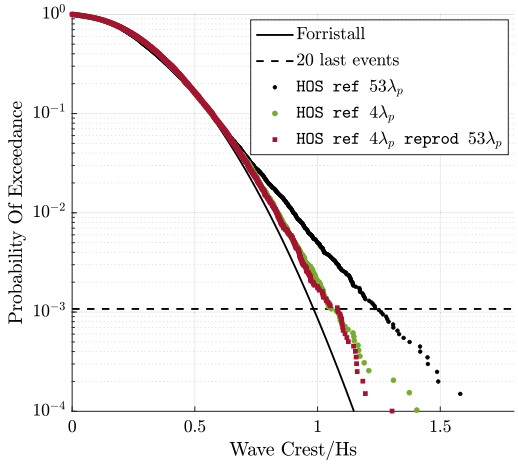

(d) HOS ref $4\lambda_p$ reprod $53\lambda_p$ crest PDER at X_t versus HOS ref $4\lambda_p$ at $X_{t_{\text{stat}}}$

Fig. 15. Comparison of HOS ref $4\lambda_p$ and HOS ref $4\lambda_p$ reprod $53\lambda_p$ generated with HOS-NWT.

Fig. 15 provides a comparison of the stochastic quantities. First, focusing on the reference wave field propagation (colored in green in the different figures), we observe that HOS ref $4\lambda_p$ is clearly qualified at $X_{t_{\text{stat}}}$. The measured significant wave height equals 100% of its target value (panel 15(a)) and the spectrum perfectly matches the ss6g5 target shape (panel 15(b)). Moreover, as expected, the crest distribution (panel 15(d)) is less extreme than the $X_{t_{\text{stat}}} = 53\lambda_p$ distributions studied in the previous subsection and plotted in black in (panel 15(d)).

The results of the new procedure for controlled statistics are shown in red lines in the different figures. It can be seen that the procedure worked well. The discrepancies observed in the time domain do not seem to affect the stochastic quantities. HOS ref $4\lambda_p$ reprod $53\lambda_p$

wave field at $X_t = 53\lambda_p$ satisfactorily reproduced both the qualified spectrum (panel 15(b)) and the crest distribution of HOS ref $4\lambda_p$ at $X_{t_{\text{stat}}} = 4\lambda_p$ (panel 15(d)).

Looking at the kurtosis evolution along the tank (panel 15(c)), we see that HOS ref $4\lambda_p$ and HOS ref $4\lambda_p$ reprod $53\lambda_p$ curves are reversed in space, as expected. For HOS ref $4\lambda_p$, the probability of the extreme events increased along the tank, as is usually observed in tank experiments, see Onorato et al. (2006) for instance. However, thanks to the time-reversal approach, for HOS ref $4\lambda_p$ reprod $53\lambda_p$, the probability of the extreme events decreases along the tank, which never occurs when using the state-of-the-art generation procedures.

As a result, the procedure for the case $X_{t_{\text{stat}}} < X_t$ is numerically validated. A non-extreme distribution and qualified spectrum were generated at $x = X_t = 53\lambda_p$ which is a location that is usually associated with extreme statistics.

6. Conclusion

A new wave generation procedure was introduced. It allows for the generation of a qualified design spectrum and a given crest distribution, at an arbitrary location in a wave tank, making use of the natural spatial evolution of the wave statistics. Two study cases were investigated. First, the procedure was successfully tested using the typical nonlinear ss6g5 design sea state studied in Canard et al. (2022b) to reproduce closer to the wave maker (at $x = 4\lambda_p$) the design spectrum and the extreme crest distribution that appears at $x = 53\lambda_p$ with the state-of-the-art procedures. Second, the procedure was successfully tested to carry out the inverse problem: generating far from the wave-maker (at $x = 53\lambda_p$) a non-extreme crest distribution that appears at $x = 4\lambda_p$ with the state-of-the-art procedures.

For both cases, the methodology relied on two main steps. First, the design spectrum was accurately generated at a location $X_{t_{\text{stat}}}$, which defined the target crest distribution. Wave maker inputs were iteratively corrected to ensure the quality of the spectrum at $X_{t_{\text{stat}}}$ (Step 1). Then, the Step 1 measurements at $X_{t_{\text{stat}}} - X_t$ (if $X_{t_{\text{stat}}} > X_t$) or $X_{t_{\text{stat}}} + X_t$ (if $X_{t_{\text{stat}}} < X_t$) were converted into inputs for the wave maker. For the case $X_{t_{\text{stat}}} < X_t$, they were also mirrored in time, to make use of the time-reversal technique. The generated wave fields reproduced between $x = 0$ and $x = X_t$ the propagation that occurred during Step 1 between $x = X_{t_{\text{stat}}} - X_t$ and $x = X_{t_{\text{stat}}}$ (if $X_{t_{\text{stat}}} > X_t$) or between $x = X_{t_{\text{stat}}} + X_t$ and $x = X_{t_{\text{stat}}}$ (if $X_{t_{\text{stat}}} < X_t$). As a result, Step 1 wave fields at $X_{t_{\text{stat}}}$ were accurately reproduced at X_t during Step 2.

For the $X_{t_{\text{stat}}} > X_t$ case, the process was conducted experimentally using the ECN Towing tank, numerically based on HOS-NWT simulations, and using a hybrid approach involving the generation of the $X_{t_{\text{stat}}}$ reference with HOS-NWT (Step 1) and its reproduction at X_t using the ECN Ocean Engineering tank (step 2). The fully experimental application of the procedure is highly time-consuming, and the final crest distribution at X_t is slightly less extreme than the $X_{t_{\text{stat}}}$ reference. The numerical and hybrid approaches are more accurate and easier to conduct. For the three cases, we have demonstrated that we can reproduce extreme wave statistics close to the wave maker, both experimentally and numerically.

For $X_{t_{\text{stat}}} < X_t$, as the procedure relies on the time reversal technique, it only works for conservative wave propagation (no dissipation). As a result, it cannot be used in the ECN Towing tank where dissipation occurs due to the side walls, nor for breaking wave conditions. In this paper we have demonstrated that we can use the procedure numerically to limit the presence of extreme events far from the wave maker.

For both $X_{t_{\text{stat}}} < X_t$ and $X_{t_{\text{stat}}} > X_t$ cases, the procedure was tested with a non-breaking unidirectional sea state. Further work will be carried out to investigate and adapt the procedure for breaking and multidirectional wave conditions. We would also point out that this procedure ensures the control of the spectrum and crest distribution only around X_t. With the case of study tested in this paper, the controlled zone does not exceed $\pm 2\lambda_p$. This is sufficient to cover the size of a structure or ship model. However, it is not sufficient for a maneuverability or towing test, where the model moves throughout the domain.

The main motivation of the present work originates from the fact that with the state-of-the-art wave generation procedures, the statistical quantities (crest PDER, kurtosis) evolve along the tank. The newly introduced procedure makes use of this spatial evolution, making it possible to reproduce at a given position the statistics that usually appear elsewhere in the tank. The study opens the way to a better control of the wave statistics in experimental and numerical wave tanks.

For now, the classification societies do not prescribe a target crest distribution or target kurtosis value. The sea state studied in this paper is unidirectional. The mechanisms behind the extreme distributions observed at the end of the basin are greatly reduced in the case of realistic short crest seas. Most of the in-situ observations show weakly non-linear statistics. However, for unstable conditions (wind changes, bathymetry variations, etc.), extreme distributions can appear. Consequently, it is of great interest to be able to control their generation in wave tanks.

CRediT authorship contribution statement

Maxime Canard: Writing – original draft, Visualization, Validation, Software, Methodology, Investigation, Data curation, Conceptualization. **Guillaume Ducrozet:** Writing – review & editing, Supervision, Software, Project administration, Methodology, Investigation, Funding acquisition, Conceptualization. **Benjamin Bouscasse:** Writing – review & editing, Supervision, Project administration, Methodology, Investigation, Funding acquisition, Conceptualization.

Declaration of competing interest

The authors declare that they have no known competing financial interests or personal relationships that could have appeared to influence the work reported in this paper.

Acknowledgments

This study was carried out in the framework of the Centrale Nantes - Bureau Veritas research chair. It was also supported by the French National Research Agency (ANR) as part of the "Investissements d'Avenir" Programme (ANR-16-IDEX-0007). We would like to thank the staff of the ECN wave tank facility Dr. Félicien Bonnefoy, Anne Levesque, Jérémy Ohana, Laurent Davoust, and Stéphane Lambert for their active help.

Appendix A. Mathematical formulation of the stochastic wave generation procedure without corrections

For both experimental and numerical wave tanks, for each realization, the wave maker takes as input a free surface elevation time-sequence, defined in the Fourier space. It corresponds to the target sequence at the wave-maker position ($x = 0$, x being the distance from the wave maker). For unidirectional wave fields, it can be expressed as:

$$\eta_{\text{input}}(t) = \sum_{n=1}^{N} A_{\text{input}_n} \cos\left(2\pi f_n t + \phi_{\text{input}_n}\right) \tag{A.1}$$

with (f_n), $n \in [1; N]$ the frequency vector and t the time. The most straightforward generation procedure uses

$$A_{\text{input}_n} = \sqrt{2 S_{\text{design}}(f_n) df} \tag{A.2}$$

with df the frequency step. And,

$$\phi_{\text{input}_n} = 2\pi U_{[0;1]} \tag{A.3}$$

$U_{[0;1]}$ being a random number following the uniform random law between 0 and 1.

Appendix B. Computation of the Benjamin Feir Index

In this paper the Benjamin Feir Index is computed following the recommendations of Serio et al. (2005), as

$$\mathrm{BFI} = \frac{k_1 H_s \sqrt{2}}{4 \nu_w} \tag{B.1}$$

with k_1 the mean wavenumber computed from the mean period

$$T_1 = \frac{\int S(f)\,\mathrm{d}f}{\int f\,S(f)\,\mathrm{d}f} \tag{B.2}$$

and ν_w the nondimensional spectral width defined with the peakedness method.

$$\nu_w = \frac{1}{Q_p \sqrt{\pi}} \tag{B.3}$$

with $Q_p = \frac{2}{(H_s^2/4)^2} \int f\,S^2(f)\,\mathrm{d}f$. Note that this definition of the BFI leads to smaller values than the one used in the famous Onorato et al. (2006) and Onorato et al. (2009) studies, where the spectral width is defined using the half width at the half maximum.

References

Annenkov, S.Y., Shrira, V., 2009. Evolution of kurtosis for wind waves. Geophys. Res. Lett. 36.

Benjamin, T.B., Feir, J.E., 1967. The disintegration of wave trains on deep water part 1. theory. J. Fluid Mech. 27, 417–430.

Bonnefoy, F., 2005. Modélisation expérimentale et numérique des états de mer complexes (Ph.D. thesis). Université de Nantes.

Brown, L.D., Cai, T.T., DasGupta, A., 2001. Interval estimation for a binomial proportion. Stat. Sci. 10, 1–117.

Bureau Veritas, 2019. NI638 guidance for long-term hydro-structure calculations.

Canard, M., Ducrozet, G., Bouscasse, B., 2022a. Generation of controlled irregular wave crest statistics in a numerical wavetank using hos-nwt solver. In: International Conference on Offshore Mechanics and Arctic Engineering. American Society of Mechanical Engineers, V05BT06A061.

Canard, M., Ducrozet, G., Bouscasse, B., 2022b. Varying ocean wave statistics emerging from a single energy spectrum in an experimental wave tank. Ocean Eng. 246, 110375.

Chabchoub, A., Fink, M., 2014. Time-reversal generation of rogue waves. Phys. Rev. Lett. 112, 124101.

Chabchoub, A., Hoffmann, N., Onorato, M., Akhmediev, N., 2012. Super rogue waves: observation of a higher-order breather in water waves. Phys. Rev. X 2, 011015.

Cherneva, Z., Tayfun, M., Guedes Soares, C., 2009. Statistics of nonlinear waves generated in an offshore wave basin. J. Geophys. Res.: Oceans 114.

Christou, M., Ewans, K., 2014. Field measurements of rogue water waves. J. Phys. Oceanogr. 44, 2317–2335.

Det Norske Veritas, 2010. Environmental conditions and environmental loads, recommended practice dnv-rp-c205.

Dommermuth, D.G., Yue, D.K., 1987. A high-order spectral method for the study of nonlinear gravity waves. J. Fluid Mech. 184, 267–288.

Ducrozet, G., Abdolahpour, M., Nelli, F., Toffoli, A., 2021. Predicting the occurrence of rogue waves in the presence of opposing currents with a high-order spectral method. Phys. Rev. Fluids 6, 064803.

Ducrozet, G., Bonnefoy, F., Mori, N., Fink, M., Chabchoub, A., 2020. Experimental reconstruction of extreme sea waves by time reversal principle. J. Fluid Mech. 884, A20.

Ducrozet, G., Bonnefoy, F., Touzé, D.Le., Ferrant, P., 2012. A modified high-order spectral method for wavemaker modeling in a numerical wave tank. Eur. J. Mech. B Fluids 34, 19–34.

Ducrozet, G., Gouin, M., 2017. Influence of varying bathymetry in rogue wave occurrence within unidirectional and directional sea-states. J. Ocean Eng. Mar. Energy 3, 309–324.

Fedele, F., Cherneva, Z., Tayfun, M., Guedes Soares, C., 2010. Nonlinear Schrödinger invariants and wave statistics. Phys. Fluids 22, 036601.

Fink, M., 1992. Time reversal of ultrasonic fields, i. basic principles. IEEE Trans. Ultrason. Ferroelectr. Freq. Control 39, 555–566.

Forristall, G.Z., 2000. Wave crest distributions: Observations and second-order theory. J. Phys. Oceanogr. 30, 1931–1943.

Fouque, J.P., Nachbin, A., 2003. Time-reversed refocusing of surface water waves. Multiscale Model. Simul. 1, 609–629.

Fouques, S., Eloïse, C., Lim, H.J., Kim, J., Canard, M., Ducrozet, G., Bouscasse, B., Koop, A., Zhao, B., Wang, W., Bihs, H., 2021. Qualification criteria for the verification of numerical waves - part 1: Potential-based numerical wave tank (pnwt). In: ASME 2021 40th International Conference on Ocean, Offshore and Arctic Engineering. American Society of Mechanical Engineers Digital Collection, V001T01A011.

Häfner, D., Gemmrich, J., Jochum, M., 2021. Real-world rogue wave probabilities. Sci. Rep. 11 (10084).

Henderson, D., Rajan, G.K., Segur, H., 2015. Dissipation of narrow-banded surface water waves. In: Hamiltonian Partial Differential Equations and Applications. Springer, pp. 163–183.

Huchet, M., Babarit, A., Ducrozet, G., Gilloteaux, J.C., Ferrant, P., 2021. Nonlinear deterministic sea wave prediction using instantaneous velocity profiles. Ocean Eng. 220, 108492.

Huo, C., Swan, C., Karmpadakis, I., Ma, L., 2023. An efficient method of defining the tail of a crest height distribution. Ocean Eng. 289, 116304.

ISO/IEC, 2008. Part 3: Guide to the expression of uncertainty in measurement.

ITTC, 2008. Guide to the expression of uncertainty in experimental hydrodynamics.

ITTC, 2011. Ittc's recommended procedures and guidelines:seakeeping experiments.

ITTC, 2017. Recommended procedures and guidelines - uncertainty analysis, instrument calibration.

Janssen, P.A., 2003. Nonlinear four-wave interactions and freak waves. J. Phys. Oceanogr. 33, 863–884.

Jensen, J.J., Capul, J., 2006. Extreme response predictions for jack-up units in second order stochastic waves by form. Probab. Eng. Mech. 21, 330–337.

Karmpadakis, I., Swan, C., 2022. A new crest height distribution for nonlinear and breaking waves in varying water depths. Ocean Eng. 266, 112972.

Karmpadakis, I., Swan, C., Christou, M., 2019. Laboratory investigation of crest height statistics in intermediate water depths. Proc. R. Soc. A 475, 20190183.

Kim, S., Bouscasse, B., Ducrozet, G., Canard, M., De Hauteclocque, G., Housseine, C.O., Ferrant, P., 2022. Numerical and experimental study of a form-based design wave applying the hos-nwt nonlinear wave solver. Ocean Eng. 263, 112287.

Kirezci, C., Babanin, A.V., Chalikov, D.V., 2021. Modelling rogue waves in 1d wave trains with the jonswap spectrum, by means of the high order spectral method and a fully nonlinear numerical model. Ocean Eng. 231, 108715.

Komen, G.J., Cavaleri, L., Donelan, M., Hasselmann, K., Hasselmann, S., Janssen, P., 1996. Dynamics and modelling of ocean waves. In: Komen, G.J., Cavaleri, L., Donelan, M., Hasselmann, K., Hasselmann, S., Janssen, PAEM (Eds.), Dynamics and Modelling of Ocean Waves. Cambridge University Press, Cambridge, UK, ISBN: 0521577810, p. 554, 554.

Latheef, M., Swan, C., 2013. A laboratory study of wave crest statistics and the role of directional spreading. Proc. R. Soc. A 469, 20120696.

Longuet-Higgins, M.S., 1952. On the statisticaldistribution of the height of sea waves. J. Mater. Res. 11, 245–266.

NWT Preparation Workgroup, 2019. Year 1 Report. Technical Report. JIP on Reproducible CFD Modeling Practice for Offshore Applications.

Onorato, M., Cavaleri, L., Fouques, S., Gramstad, O., Janssen, P.A., Monbaliu, J., Osborne, A.R., Pakozdi, C., Serio, M., Stansberg, C., et al., 2009. Statistical properties of mechanically generated surface gravity waves: a laboratory experiment in a three-dimensional wave basin. J. Fluid Mech. 627, 235–257.

Onorato, M., Osborne, A.R., Serio, M., Cavaleri, L., Brandini, C., Stansberg, C., 2006. Extreme waves, modulational instability and second order theory: wave flume experiments on irregular waves. Eur. J. Mech. B Fluids 25, 586–601.

Ransley, E.J., Brown, S.A., Hann, M., Greaves, D.M., Windt, C., Ringwood, J., Davidson, J., Schmitt, P., Yan, S., Wang, J.X., et al., 2021. Focused wave interactions with floating structures: A blind comparative study. Proc. Inst. Civ. Eng.-Eng. Comput. Mech. 174, 46–61.

Seiffert, B.R., Ducrozet, G., 2018. Simulation of breaking waves using the high-order spectral method with laboratory experiments: wave-breaking energy dissipation. Ocean Dyn. 68, 65–89.

Seiffert, B.R., Ducrozet, G., Bonnefoy, F., 2017. Simulation of breaking waves using the high-order spectral method with laboratory experiments: Wave-breaking onset. Ocean Model. 119, 94–104.

Serio, M., Onorato, M., Osborne, A.R., Janssen, P.A., 2005. On the computation of the Benjamin-Feir Index. Il Nuovo Cimento C 28, 893–903.

Suret, P., Tikan, A., Bonnefoy, F., Copie, F., Ducrozet, G., Gelash, A., Prabhudesai, G., Michel, G., Cazaubiel, A., Falcon, E., et al., 2020. Nonlinear spectral synthesis of soliton gas in deep-water surface gravity waves. Phys. Rev. Lett. 125, 264101.

Tang, T., Adcock, T.A., 2021. The influence of finite depth on the evolution of extreme wave statistics in numerical wave tanks. Coast. Eng. 166, 103870.

Tayfun, M.A., 1990. Distribution of large wave heights. J. Waterw. Port Coast. Ocean Eng. 116, 686–707.

Tayfun, M.A., Fedele, F., 2007. Wave-height distributions and nonlinear effects. Ocean Eng. 34, 1631–1649.

Toffoli, A., Alberello, A., Clarke, H., Nelli, F., Benetazzo, A., Bergamasco, F., Ntamba, B.N., Vichi, M., Onorato, M., 2024. Observations of rogue seas in the southern ocean. Phys. Rev. Lett. 132, 154101.

Tromans, P.S., Anaturk, A.R., Hagemeijer, P., 1991. A new model for the kinematics of large ocean waves-application as a design wave. In: The First International Offshore and Polar Engineering Conference. OnePetro, pp. ISOPE–I–91–154.

van Essen, S.M., Scharnke, J., Seyffert, H.C., 2023. Required test durations for converged short-term wave and impact extreme value statistics—part 1: Ferry dataset. Mar. Struct. 90, 103410.

Welch, P., 1967. The use of fast fourier transform for the estimation of power spectra: a method based on time averaging over short, modified periodograms. IEEE Trans. Audio Electroacoust. 15, 70–73.

West, B.J., Brueckner, K.A., Janda, R.S., Milder, D.M., Milton, R.L., 1987. A new numerical method for surface hydrodynamics. J. Geophys. Res.: Oceans 92, 11803–11824.

Xie, C.M., Yang, J.C., Sun, P.N., Lyu, H.G., Yu, J., Ye, Y.L., 2023. An accurate and efficient hos-meshfree cfd coupling method for simulating strong nonlinear wave–body interactions. Ocean Eng. 287, 115889.

Zve, E., Swan, C., Hughes, G., 2023. Crest-height statistics in finite water depth. part 1: The role of the nonlinear interactions in uni-directional seas. Ocean Eng. 289, 116369.